Title	Highly spin-polarized carrier dynamics and ultra-large photoinduced magnetization in CH3NH3PbI3 perovskite thin films
Author(s)	Giovanni, David; Ma, Hong; Chua, Julianto; Grätzel, Michael; Ramesh, Ramamoorthy; Mhaisalkar, Subodh; Mathews, Nripan; Sum, Tze Chien
Citation	Giovanni, D., Ma, H., Chua, J., Grätzel, M., Ramesh, R., Mhaisalkar, S., et al. (2015). Highly spin-polarized carrier dynamics and ultra-large photoinduced magnetization in CH3NH3PbI3 perovskite thin films. Nano letter, 5 (3), 1553–1558.
Date	2015
URL	http://hdl.handle.net/10220/25022
Rights	

Highly Spin-polarized Carrier Dynamics and Ultra-large Photoinduced Magnetization in CH$_3$NH$_3$PbI$_3$ Perovskite Thin Films

David Giovanni[1,2], Hong Ma[1,3], Julianto Chua[2,4], Michael Grätzel[2,5], Ramamoorthy Ramesh[6], Subodh Mhaisalkar[2,4], Nripan Mathews[2,4*] and Tze Chien Sum[1*]

1. Division of Physics and Applied Physics, School of Physical and Mathematical Sciences, Nanyang Technological University, 21 Nanyang Link, Singapore 637371, Singapore.

2. Energy Research Institute @NTU (ERI@N), Research Techno Plaza, X-Frontier Block, Level 5, 50 Nanyang Drive, Singapore 637553, Singapore.

3. College of Physics and Electronics, Shandong Normal University, 88 East Wenhua Road, Jinan 250014, P. R. China

4. School of Materials Science and Engineering, Nanyang Technological University, Nanyang Avenue, Singapore 639798, Singapore.

5. Laboratory of Photonics and Interfaces, Department of Chemistry and Chemical Engineering, Swiss Federal Institute of Technology, Station 6, CH-1015 Lausanne, Switzerland.

6. Department of Materials Science and Engineering, 210 Hearst Memorial Mining Building, University of California, Berkeley, CA 94720

Abstract:

Low temperature solution-processed organic-inorganic halide perovskite $CH_3NH_3PbI_3$ has demonstrated great potential for photovoltaics and light emitting devices. Recent discoveries of long ambipolar carrier diffusion lengths and the prediction of the Rashba effect in $CH_3NH_3PbI_3$, that possesses large spin-orbit coupling, also point to a novel semiconductor system with highly promising properties for spin-based applications. Through circular pump-probe measurements, we demonstrate that highly polarized electrons of total angular momentum (J) with an initial degree of polarization P_{ini} ~ 90% (*i.e.*, −30% degree of electron spin polarization) can be photogenerated in perovskites. Time-resolved Faraday rotation measurements reveal photo-induced Faraday rotation as large as 10°/μm at 200 K (at wavelength λ = 750 nm) from an ultrathin 70 nm film. These spin polarized carrier populations generated within the polycrystalline perovskite films, relax via intraband carrier spin-flip through the Elliot-Yafet mechanism. Through a simple two-level model, we elucidate the electron spin relaxation lifetime to be ~7 ps and that of the hole is ~1 ps. Our work highlights the potential of $CH_3NH_3PbI_3$ as a new candidate for ultrafast spin switches in spintronics applications.

Keywords: spintronics, circular pump-probe, spin polarization, spin dynamics, Faraday rotation.

Low-temperature solution-processed organic-inorganic halide perovskites such as $CH_3NH_3PbI_3$, have recently emerged as the forerunner material in 3rd generation photovoltaic technologies with efficiencies approaching 20%.[1] The origins of their high efficiencies stem from their high absorption coefficients[2] and long range ambipolar carrier diffusion lengths[3]. Surprisingly, this family of halide perovskites was also found to exhibit excellent optical gain and light emitting properties.[4] Density functional theory studies not only showed that the band structure of $CH_3NH_3PbI_3$ is strongly modulated by a giant spin orbit coupling (SOC)[2,5] in the conduction band, but also recently predicted the presence of a Rashba-type splitting in $CH_3NH_3PbI_3$.[6] These discoveries denote a novel semiconductor system with highly promising characteristics for spin-based applications. Nevertheless, studies on spin phenomena in halide perovskites are still very limited. While on the one hand, possessing a large SOC is desirable for spin injection, on the other hand a large SOC can also severely limit the spin relaxation lifetimes.[7] Detailed studies on elucidating the spin dynamics and understanding the dominant relaxation mechanisms[7] are therefore urgently needed to assess its suitability for spin-based applications.

Spin relaxation lifetimes are typically described using the characteristic times of T_1 (also known as longitudinal spin relaxation time or spin-lattice relaxation time) and T_2* (also known as ensemble transverse spin relaxation time or spin decoherence time). Herein, we focus on elucidating T_1 using circular pump-probe techniques without any external applied magnetic field. From earlier studies, it has been shown that in the absence of SOC, $CH_3NH_3PbI_3$ would have a direct bandgap at R point which consist of a six-fold degenerate $J = 1/2$ and $3/2$ ($L = 1$) conduction band (CB) and doubly degenerate $J = 1/2$ ($L = 0$) upper valence band (VB).[2,5,8] However, with SOC, the CB is split into a doubly degenerate lower $J = 1/2$ band (~1.6 eV from

the VB maximum – which corresponds to the bandgap) and an upper four-fold degenerate $J =$ 3/2 band (~2.8 eV from the VB maximum), where J is the total angular momentum quantum number. The upper VB is however unaffected by the SOC – Figure 1(a).[2, 5] Here, we limit our study to near bandgap excitation, *i.e.* the upper VB and lower CB.
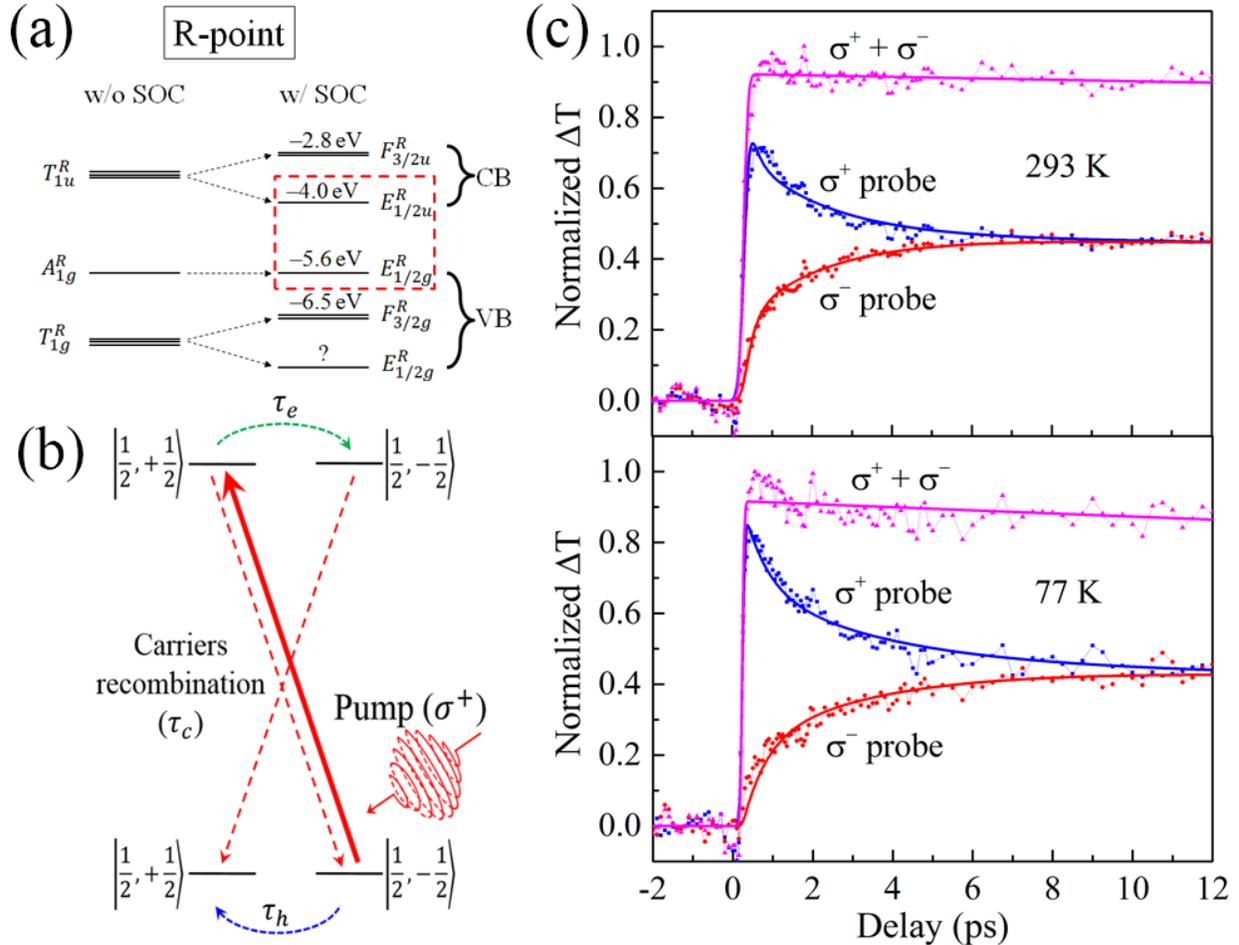

Figure 1: (a) Energy bands of $CH_3NH_3PbI_3$ at R-point (point group symmetry representation)[5] with their respective levels from vacuum (experimental).[2-3] Dashed box indicates the bands of interest. (b) Model of near band-edge photoexcitation by σ^+ photon and J-states dynamics of $CH_3NH_3PbI_3$. The state notation is written as $|J, m_J\rangle$ where J = ½ is electron's total angular momentum quantum number and m_J = ±½ is its projection in the z-axis. Absorption of σ^+ pump will raise the angular momentum by $+\hbar$ (Δm_j = +1). (c) Normalized circular pump-probe decay transients with 19 µJ/cm^2 σ^+ pump and σ^+ probe (blue), σ^- probe (red) and their total (magenta), at 293 K (top) and 77 K (bottom). The experimental data is globally fitted using eq. 3 (σ^+ probe and σ^- probe) and eq. 4 (their total). (a) adapted with permission from ref [5]. Copyright (2014) American Chemical Society.

From this band-structure, we envisage that instantaneous excitations of near 100% *J*-polarized populations of carriers (constituting about –33% spin-polarized electrons – see discussion below) in $CH_3NH_3PbI_3$ can be generated using 1.65 eV left circularly-polarized pump pulses (σ^+_{pump}, by the spectroscopists' convention of being from the receiver's/detector's point of view)[9] resonantly tuned above $CH_3NH_3PbI_3$'s direct bandgap of 1.63 eV. The negative sign for the electrons degree of polarization indicates a spin polarization alignment counter-polarized to the direction of injected angular momentum $+\hbar$ (see details in Supporting Info). As the σ^+ photon carries an angular momentum of $+\hbar$ (in the direction of propagation), the absorption of such a photon will raise the angular momentum by $+\hbar$ ($\Delta m_j = +1$), in accordance with total angular momentum conservation. While the circularly polarized pump defines the spin orientation of the carriers in the sample, each probe polarization will trace the different m_j states. In the later part, these $m_j = \pm\frac{1}{2}$ states will be referred as "*J*-states". Tracking the changes to the *J*-polarized carrier populations in time with left (σ^+_{probe}) or right (σ^-_{probe}) circularly polarized probe pulses will allow us to elucidate the dynamics of the electron/hole angular momentum flip and also model these dynamics with a simple two-level system. Note that $m_j = +\frac{1}{2}$ ($-\frac{1}{2}$) state in the CB corresponds to 1:2 mixtures of spin states with azimuthal number $m_s = +\frac{1}{2}$ and $-\frac{1}{2}$ ($-\frac{1}{2}$ and $+\frac{1}{2}$); while the *J*-states are same as the spin states ($m_j = m_s$) for the VB, as shown by eq. 1:

$$\left| L, S, J, m_j \right\rangle = \sum_{m_l} \sum_{m_s} \left\langle L, S, m_l, m_s \mid L, S, J, m_s \right\rangle \left| L, S, m_l, m_s \right\rangle$$

$$\left| 1, \tfrac{1}{2}, \tfrac{1}{2}, \pm\tfrac{1}{2} \right\rangle_{CB} = \mp\sqrt{\tfrac{1}{3}} \left| 1, \tfrac{1}{2}, 0, \pm\tfrac{1}{2} \right\rangle \pm \sqrt{\tfrac{2}{3}} \left| 1, \tfrac{1}{2}, \pm 1, \mp\tfrac{1}{2} \right\rangle \tag{1}$$

$$\left| 0, \tfrac{1}{2}, \tfrac{1}{2}, \pm\tfrac{1}{2} \right\rangle_{VB} = \left| 0, \tfrac{1}{2}, 0, \pm\tfrac{1}{2} \right\rangle.$$

This can be deduced from the Clebsch-Gordan coefficients for a system with *L* and *S* coupling. We show that the electron's degree of spin-polarization is −⅓ of electron's degree of *J*-polarization in CB; while for hole in VB, *J* = *S*.

Our findings reveal that the highly *J*-polarized electrons relaxes within 10 ps, while the holes relax on a much faster 1 ps timescale in the polycrystalline $CH_3NH_3PbI_3$ thin film. Note that since each *J*-state comprises of a unique ratio of the spin-states, *J*-state relaxation also represents spin-state relaxation – details in Supporting Info. Temperature dependent and pump fluence dependent measurements indicate that the dominant *J*-states relaxation channel is the intraband spin-flip through Elliot-Yafet (EY) mechanism. Time-resolved Faraday rotation measurements uncovered a high degree of photoinduced Faraday rotation as large as 720 milli-degrees (at wavelength, λ = 750 nm) from a 70 nm (± 10 nm) ultrathin $CH_3NH_3PbI_3$ polycrystalline film (*i.e.*, corresponding to 10°/μm ± 2°/μm, proportional to *J*-polarization). Comparatively, this value is higher than that for a 0.5 μm thick bismuth iron garnet ($Bi_3Fe_5O_{12}$) film which is ~6°/μm at λ= 633 nm.[10] These findings highlight the potential of $CH_3NH_3PbI_3$ for application as ultrafast spin switches in spintronics.[11]

Our samples comprises of 70 ± 10 nm-thick solution-processed $CH_3NH_3PbI_3$ films spin-coated on a quartz substrate. Details on the sample preparation and thickness measurements can be found in the Supporting Info. Temperature and fluence dependent degenerate pump-probe at 750 nm (1.65 eV) slightly above the absorption band edge (~1.63 eV) were performed using ~50 fs laser pulses, with both pump and probe focused into ~260 μm diameter spot. Three different pump polarizations were used for each measurement (right circular σ^-, linear σ^0 and left circular σ^+) to verify the observation of *J*-states dynamics, while the linear probe polarization

was then separated into two equal components of left and right circular polarization by a quarter wave-plate and Wollaston prism for separate detection. Each probe polarization will trace the different J-states. Experimental details and the verifications on the circular pump-probe setup can also be found in the Supporting Info.

To gain more insights into the non-equilibrium J-states relaxation mechanism and to decouple the electron and hole J-relaxation times, we utilize a kinetic model based on a two-level system as shown in Figure 1(b). The population kinetics of the electrons (holes) in a given $\left|J, m_j\right\rangle$-state in conduction (valence) band can be described by the following rate equation:

$$\frac{d}{dt} f_{e,h}^{|1/2,\pm1/2\rangle} = A\left(\frac{1\pm p}{2}\right)e^{-t^2/\tau_0^2} - \frac{f_{e,h}^{|1/2,\pm1/2\rangle} - f_{e,h}^{|1/2,\mp1/2\rangle}}{\tau_{e,h}} - \frac{f_{e,h}^{|1/2,\pm1/2\rangle}}{\tau_c} \qquad (2)$$

where $f_e^{|1/2,\pm1/2\rangle}$ ($f_h^{|1/2,\pm1/2\rangle}$) denotes electrons (holes) occupation probability for a given electron $\left|J, m_j\right\rangle$-state in CB (VB), τ_0 is laser temporal pulse width parameter (Gaussian pulse), p is the excitation degree of polarization which is equal to 1 for pure circular excitation as in our case, τ_e (τ_h) is the electrons (holes) J relaxation time, $i.e.$, intraband interstates transfer time or 'J-flip' (correspond to spin-flip), which is related to T_1 through $2T_1 = \tau_{e,h}$, and τ_c is the spin-independent carrier relaxation time. Here, T_1 can be related to J relaxation time because J-polarization is directly proportional to the spin-polarization; hence they share identical relaxation times. Note that $f_h^{|1/2,\mp1/2\rangle}$ in VB refers to the hole state with $m_j = \pm\frac{1}{2}$.[12] Due to the dynamics of state filling, the pump-probe signal is proportional to the sum of the electron and hole occupation populations, which can be written as:

$$\left(\frac{\Delta T}{T}\right)_{\pm\frac{1}{2}} \propto f_e^{\pm\frac{1}{2}} + f_h^{\mp\frac{1}{2}}. \tag{3}$$

Eqn. 2 can be solved analytically to obtain the following fitting function:

$$\left(\frac{\Delta T}{T}\right)_{\pm\frac{1}{2}} \propto e^{-t/\tau_c} \left\{ \left[1+\mathrm{erf}\left(\frac{t}{\tau_0} - \frac{\tau_0}{2\tau_c}\right) \right] \pm \frac{1}{2}\sum_{i=e,h}\left[e^{\tau_0^2/\tau_i^2}\left(1+\mathrm{erf}\left(\frac{t}{\tau_0} - \frac{\tau_0}{\tau_i}\right)\right)e^{-2t/\tau_i} \right] \right\}. \tag{4}$$

The experimental data is then globally fitted (simultaneously) by using eqn. 4 with +½ and –½ for σ^+ and σ^- probe signal respectively, to obtain the shared fitting parameter values. Note that when the signal from σ^+ probe and σ^- probe are added up, the result will be the total number of carriers in both J-states and is independent of the pump polarization as shown in eqn. 5:

$$\left(\frac{\Delta T}{T}\right)_{+\frac{1}{2}} + \left(\frac{\Delta T}{T}\right)_{-\frac{1}{2}} \propto \left[1+\mathrm{erf}\left(\frac{t}{\tau_0} - \frac{\tau_0}{2\tau_c}\right) \right] e^{-t/\tau_c} \tag{5}$$

Figure 1(c) shows that the experimental data (at 293 K and 77 K) for σ^+ pump excitation (with fluence of 19 µJ/cm^2) are well-fitted using eqn. 4. Following σ^+ pump excitation, the σ^+ probe signal (blue data points) first exhibits a sharp rise (indicating a large photoexcited population of electrons in the $m_j = +½$ J-state), which then proceeds with a decay of the signal to equilibrium (signifying the depopulation of $m_j = +½$ state). Concomitantly, the σ^- probe signal (red data points) rises gradually (indicating the filling of $m_j = -½$ state) at a rate that matches the decay of the σ^+ probe signal. In the absence of any external magnetic field, the J-polarized electrons approach to an equilibrium with 50% 'J-up' ($m_j = +½$ state) and 50% 'J-down' ($m_j = -½$ state). These equalized populations of electrons and holes eventually undergo carrier recombination on a nanosecond timescale typical for the $CH_3NH_3PbI_3$ system.[3] The sum of the

σ^+ and σ^- probe signals (magenta data points), which shows a sharp rise and continued by an approximately constant value within the measurement time window, is also well-fitted eqn. 5 – thus validating our preceding discussion on the total number of photoexcited carriers. This result clearly shows that the *J* state-relaxation occurs in a timescale much shorter than the carrier recombination lifetime ($\tau_{e,h} \square \ \tau_c$), consistent with an intraband population transfer between the two *J*-states *i.e.*, intraband angular momentum flip (*J*-flip). The intraband *J*-flip process stops after the populations between these two states are balanced.

Although a 100% *J*-polarized signal is expected from the selection rules, the maximum σ^+ probe signals in <u>Figure 1(b)</u> immediately after photoexcitation is only about 70% at 293K (or ~80% at 77K), much lower than the total carrier population ($\sigma^+ + \sigma^-$). This indicates that only such fraction of the photoexcited carriers occupy the +½ m_j-state. We attributed this to the ultrafast hole spin relaxation process, which occurs much faster than that of the electrons[12], and is comparable to the timescale of our excitation pulse. This is evident from the deconvolution of the electron and hole contributions at 77 K as shown in <u>Figure 2(a)</u> (see Supporting Information for details of the method). <u>Figure 2(a)</u> shows the plots of population difference between $m_j = $ +½ and $m_j = $ –½ states at 77 K for both electrons ($\Delta f_e = f_e^{+1/2} - f_e^{-1/2}$) and holes ($\Delta f_h = f_h^{-1/2} - f_h^{+1/2}$) and that of the difference between the σ^+ and σ^- probe signals (*i.e.*, $\sigma^+ - \sigma^-$). The latter is in fact equals to the difference between total population of $m_j = $ +½ and $m_j = $ –½ states of both electron and hole, *i.e.*, $\Delta f_e + \Delta f_h$. Using the common definition for degree of spin polarization (η),[7, 12-13] we defined the parameters:

$$\eta_{\text{electrons}}(t) = \frac{N_{e\uparrow} - N_{e\downarrow}}{N_{e\uparrow} + N_{e\downarrow}} = -\frac{\Delta f_e}{3 f_e}$$

$$\eta_{\text{holes}}(t) = \frac{N_{h\uparrow} - N_{h\downarrow}}{N_{h\uparrow} + N_{h\downarrow}} = \frac{\Delta f_h}{f_h}$$

(6)

for electrons and holes – plotted in <u>Figure 2(b)</u>, for a time delay 0.5 ps after laser excitation where the signal rise is cut off (to minimize the effects of backscattered laser light from the sample). $N_\uparrow$ and $N_\downarrow$ denotes the population of spin-up ($m_s = +\frac{1}{2}$) and spin-down ($m_s = -\frac{1}{2}$) respectively. From the figure, the initial degree of electrons spin polarization P_{ini} is about -30% (90% J-polarization), which agrees with our initial expectation. The electron spin decays on a much longer time scale of 7 ± 1 ps compared to that of the holes 1.1 ± 0.1 ps.
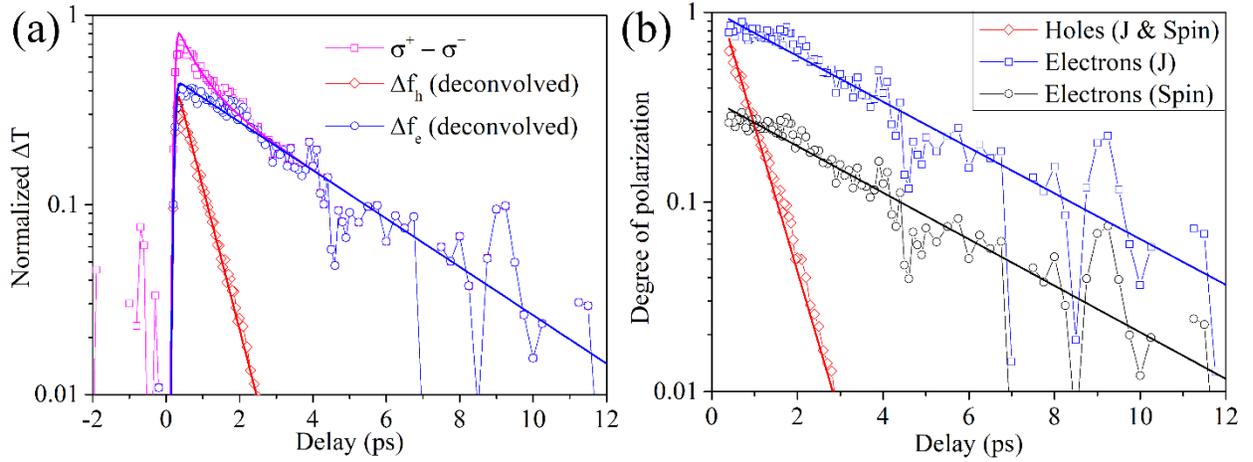

Figure 2: Experimental data with 19 μJ/cm^2 pump at 77 K. (a) The difference between σ^+ and σ^- signal (magenta) is plotted together with the deconvoluted contribution from electrons (blue) and holes (red). Δf_e (Δf_h) denotes the population difference between spin-up and spin-down electrons (holes). (b) The degree of polarization dynamics after 0.5 ps of holes for spin and J (red), electrons J (blue) and electrons spin (black, absolute value).

Circular pump probe measurements were also performed as a function of temperature and fluence to elucidate the J-relaxation mechanism (corresponds to spin-relaxation and has identical relaxation time). <u>Figure 3(a)</u> shows temperature dependence of spin relaxation time for both electrons and holes, obtained from fits using eqn. 4 (within $\pm 10\%$ accuracy) at a pump fluence of

$19~\mu J/cm^2$. The result shows that for electrons the spin relaxation time generally decreases with increasing temperature, but exhibits a weak dependence on temperature as the spin lifetimes decreases by factor ~1.6 across the temperature range. Although the holes spin relaxation time show a similar decreasing trend with temperature, it is in fact more susceptible to temperature effects (as the decrease is about two times larger).
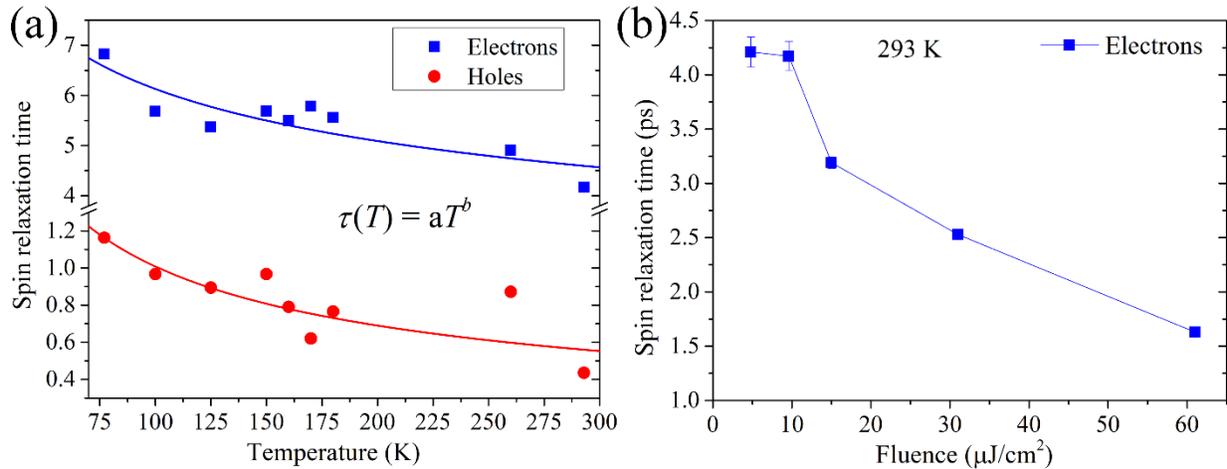

Figure 3: Measured spin relaxation time of electrons (blue) and holes (red) as (a) temperature dependence fitted with $\tau \propto T^b$ where we obtain $b = -0.27 \pm 0.06$ for electrons and $b = -0.55 \pm 0.15$ for holes and (b) fluence dependence (for electrons). Holes spin relaxation time at high fluence is shorter than our temporal resolution and hence cannot be measured.

Amongst the three possible spin relaxation mechanisms, only the Elliott-Yafet (EY) mechanism is most probable for $CH_3NH_3PbI_3$. The D'yakonov-Perel' (DP) mechanism, which is applicable to systems without inversion symmetry[7], is irrelevant because the $CH_3NH_3PbI_3$ crystal structure exhibits inversion symmetry. The Bir-Aronov-Pikus (BAP) mechanism, which is applicable to heavily p-doped semiconductor[7], is also unlikely as our sample does not contain significant amounts of p-doping. Moreover, BAP relaxation rate depends on the exchange interaction between electrons and holes which generally can be characterized through the exchange (hyperfine) splitting of excitonic ground state.[7, 14] However this splitting has never

been observed in $CH_3NH_3PbI_3$, plausibly because it is very weak. Hence, we believe that in our case, BAP does not play an important role in the spin-flip processes.

From its weak dependence on temperature, we infer that the spin relaxation occurs mainly through Elliott-Yafet (EY) impurities and grain boundaries scattering. We substantiate this assignment with the power fits of $\tau \propto T^b$ for spin relaxation time vs temperature, where we obtained $b = -0.27 \pm 0.06$ for electrons and $b = -0.55 \pm 0.15$, which is close to the theoretical prediction $\tau \propto T^{-1/2}$ of EY mechanism for scattering by charged impurities.[7] Figure 3(b) shows the fluence dependent electrons spin relaxation time measurement as function of pump fluence at 293 K. Note that holes spin relaxation time at high fluence is shorter than our temporal resolution. The result shows a strong dependence with decreasing trend of spin relaxation time with the increasing fluence especially at high fluence, which implies that carrier-carrier scattering also contributes to the spin relaxation process. As the spin flip process originates mainly from carriers, impurities and grain boundaries scattering, longer spin diffusion lengths can be expected from vacuum-deposited $CH_3NH_3PbI_3$ samples at room temperatures, instead of solution-processed samples in this work. Furthermore, it should also be feasible to tune the SOC through the replacement of the A cation, *i.e.*, Pb with other transition metals such as Cu and Sn. This could possibly lead to longer spin diffusion lengths at room temperatures.

Lastly, time-resolved Faraday rotation (TRFR) measurements as a function of temperature (in zero magnetic field) were also performed to examine the photoinduced magnetization from the $CH_3NH_3PbI_3$ thin films. Figure 4(a) shows a typical pump-induced Faraday rotation signal taken at 75 K for σ^+, σ^- and σ^0 (linear) pump excitations at 750 nm wavelength. Details on the TRFR setup and measurements are given in the Supporting Info. The sign inversion of the Faraday rotation signals for opposite circular polarizations of the pump beam and null signal

from the linear pump excitation help validate that the photoinduced magnetization is observed. Here, the rotation angle is proportional to sample's magnetization,[7, 14-15] which originates from the photoinduced carrier J-polarization (*i.e.* $\propto \Delta f_e + \Delta f_h$). No signal was observed from blank quartz substrate. Bi-exponential fitting yields the lifetimes $\tau_1 = 0.9 \pm 0.1$ ps (holes) and $\tau_2 = 4 \pm 1$ ps (electrons), which are consistent with the values obtained from the J-flip (or spin-flip) measurements ($\tau_h = \sim1.1$ ps for holes and $\tau_e = \sim7$ ps for electrons). Note that magnetization lifetime is expected to be half of spin-flip lifetime, since it measures the population difference between both spin states, which doubles the rate – (for details see Supporting Info).
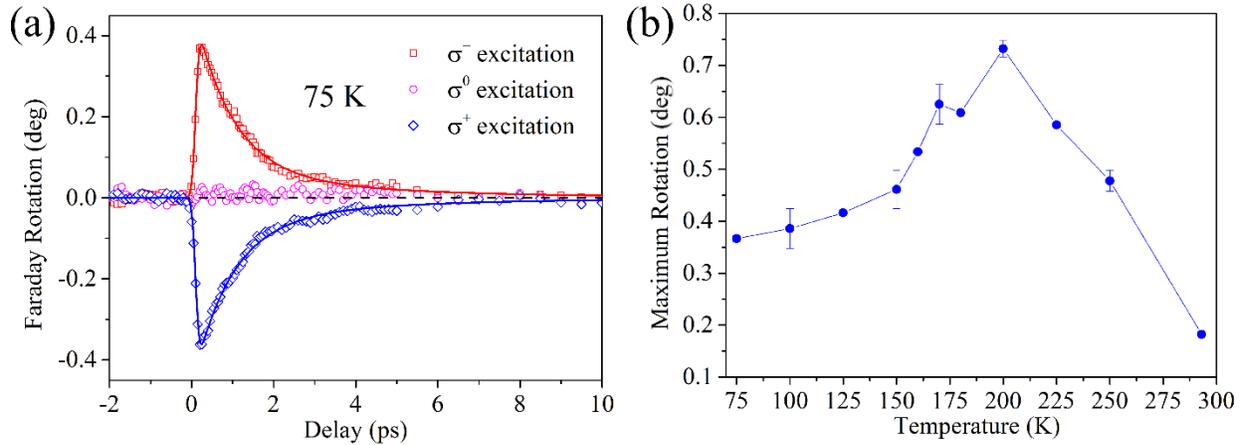

Figure 4: TRFR study on $CH_3NH_3PbI_3$ at fluence 19 µJ/cm^2. (a) Typical signal of pump-induced Faraday rotation which is proportional to sample magnetization, fitted with a bi-exponetial decay function ($\tau_1 = 0.9 \pm 0.1$ ps and $\tau_2 = 4 \pm 1$ ps). Switching pump polarization between σ^+ and σ^- will flip the signal, while no rotation is observed for σ^0 polarization. (b) Maximum rotation (peak) as function of temperature.

It is remarkable that a very large pump-induced Faraday rotation of ~720 milli-degrees (mdeg) at 200 K is obtained from these nanometric thick (*i.e.*, 70 ± 10 nm) $CH_3NH_3PbI_3$ films (*i.e.*, 10°/µm ± 2°/µm)– Figure 4(b). Comparatively, this value is higher than that for a 0.5 µm thick bismuth iron garnet film ($Bi_3Fe_5O_{12}$) which has ~6°/µm at room temperature (at wavelength 633 nm),[10] thick drop-casted (few microns thick) colloidal CdSe quantum dots with cavity

enhancement of Faraday rotation at room temperature (~350 mdeg at wavelength 630 nm);[16] and much higher that the ~1 μm-thick MnSe Digital Magnetic Heterostuctures (DMH) at 5 K (~0.6°/μm at wavelength 440-510 nm).[15] Such ultra-large photoinduced magnetization is characteristic of the large SOC from $CH_3NH_3PbI_3$. Temperature dependence of the TRFR signal is given in Figure 4(b), where the trend is most likely related to the phase transitions of $CH_3NH_3PbI_3$.

In summary, we report on the first spin dynamics studies in $CH_3NH_3PbI_3$ using spin-dependent circularly-polarized pump-probe techniques. Our findings show that the *J*-states (or spin) relaxation in $CH_3NH_3PbI_3$ occurs through intraband (*J*-flips) spin flips within 10 ps (for electrons) and 1 ps (for holes) as validated by a simple two-state model. The dominant spin relaxation is believed to be the EY impurities scattering mechanism. TRFR measurements uncovered a high degree of photoinduced Faraday rotation as large as 720 mdeg from an ultrathin ~70 nm $CH_3NH_3PbI_3$ polycrystalline thin film (*i.e.*, 10°/μm ± 2°/μm). Comparatively, this value is much higher than that for magnetic heterostuctures of equivalent thicknesses. Importantly, our work highlights the potential of $CH_3NH_3PbI_3$ as a new candidate for Spintronics applications especially as ultrafast spin switches. While current findings suggest some limitations in solution-processed $CH_3NH_3PbI_3$ thin-film for spin-transport purposes due to fast spin relaxation, there are, nonetheless possibilities to overcome such shortcomings through improvements in sample preparation techniques, *e.g.*, vacuum deposition, or through materials engineering, such as both cation and anion replacement in such perovskites, which could be further explored as means to tune the SOC.

ASSOCIATED CONTENT

Supporting Information

Details of sample preparation; measurement of film thickness; detailed analysis of band structure, *J*-states and spin-states; experimental procedures and verification of circular pump probe; detailed mathematical derivation for the model; detailed experimental procedures of TRFR. This material is available free of charge via the Internet at http://pubs.acs.org.

AUTHOR INFORMATION

Corresponding Authors:

*N.M.: Email: Nripan@ntu.edu.sg

*T.C.S.: Email: Tzechien@ntu.edu.sg

ACKNOWLEDGEMENT

REFERENCES:

1.   Zhou, H.; Chen, Q.; Li, G.; Luo, S.; Song, T.-b.; Duan, H.-S.; Hong, Z.; You, J.; Liu, Y.; Yang, Y., Interface engineering of highly efficient perovskite solar cells. *Science* **2014,** *345* (6196), 542-546.

2.   Tanaka, K.; Takahashi, T.; Ban, T.; Kondo, T.; Uchida, K.; Miura, N., Comparative study on the excitons in lead-halide-based perovskite-type crystals $CH_3NH_3PbBr_3$ $CH_3NH_3PbI_3$. *Solid State Communications* **2003,** *127* (9–10), 619-623.

3.   Xing, G.; Mathews, N.; Sun, S.; Lim, S. S.; Lam, Y. M.; Grätzel, M.; Mhaisalkar, S.; Sum, T. C., Long-Range Balanced Electron- and Hole-Transport Lengths in Organic-Inorganic CH3NH3PbI3. *Science* **2013,** *342* (6156), 344-347.

4.   Xing, G.; Mathews, N.; Lim, S. S.; Yantara, N.; Liu, X.; Sabba, D.; Grätzel, M.; Mhaisalkar, S.; Sum, T. C., Low-temperature solution-processed wavelength-tunable perovskites for lasing. *Nat Mater* **2014,** *13* (5), 476-480.

5.   Even, J.; Pedesseau, L.; Katan, C., Analysis of Multivalley and Multibandgap Absorption and Enhancement of Free Carriers Related to Exciton Screening in Hybrid Perovskites. *The Journal of Physical Chemistry C* **2014,** *118* (22), 11566-11572.

6.   Kim, M.; Im, J.; Freeman, A. J.; Ihm, J.; Jin, H., Switchable S = 1/2 and J = 1/2 Rashba bands in ferroelectric halide perovskites. *Proceedings of the National Academy of Sciences* **2014,** *111* (19), 6900-6904.

7.   Zutic, I.; Fabian, J.; Das Sarma, S., Spintronics: Fundamentals and applications. *Reviews of Modern Physics* **2004,** *76* (2), 323-410.

8.   Umebayashi, T.; Asai, K.; Kondo, T.; Nakao, A., Electronic structures of lead iodide based low-dimensional crystals. *Physical Review B* **2003,** *67* (15), 155405.

9.   Kimball, D. F. J.; Alexandrov, E. B.; Budker, D., General Principles and Characteristics of Optical Magnetometers In *Optical Magnetometry*, Dmitry Budker , D. F. J. K., Ed. Cambridge University Press: Cambridge, 2013; pp 1-24.

10.   Kahl, S.; Popov, V.; Grishin, A. M., Optical transmission and Faraday rotation spectra of a bismuth iron garnet film. *Journal of Applied Physics* **2003,** *94* (9), 5688-5694.

11.   Takahashi, R., Low-temperature-grown surface-reflection all-optical switch (LOTOS). *Optical and Quantum Electronics* **2001,** *33* (7-10), 999-1017.

12.   Dyakonov, M. I., Basics of Semiconductor and Spin Physics. In *Spin Physics in Semiconductors*, Dyakonov, M., Ed. Springer Berlin Heidelberg: 2008; Vol. 157, pp 1-28.

13.   Holub, M.; Bhattacharya, P., Spin-Polarized Light-Emitting Diodes and Lasers. *Journal of Physics D: Applied Physics* **2007,** *40* (11), R179.

14.   Wu, M. W.; Jiang, J. H.; Weng, M. Q., Spin dynamics in semiconductors. *Physics Reports* **2010,** *493* (2–4), 61-236.

15.   Crooker, S. A.; Awschalom, D. D.; Samarth, N., Time-resolved Faraday rotation spectroscopy of spin dynamics in digital magnetic heterostructures. *Selected Topics in Quantum Electronics, IEEE Journal of* **1995,** *1* (4), 1082-1092.

16.   Li, Y. Q.; Steuerman, D. W.; Berezovsky, J.; Seferos, D. S.; Bazan, G. C.; Awschalom, D. D., Cavity enhanced Faraday rotation of semiconductor quantum dots. *Applied Physics Letters* **2006,** *88* (19), 193126.

Table of Content Graphics: